JOURNAL OF PROPULSION AND POWER
Vol. 12, No. 3, May–June 1996

Computational Study of Viscous Effects on Lobed Mixer Flow Features and Performance

M. N. O'Sullivan,* J. K. Krasnodebski,* I. A. Waitz,† E. M. Greitzer,‡ and C. S. Tan§
Massachusetts Institute of Technology, Cambridge, Massachusetts 02139
and
W. N. Dawes¶
Cambridge University, Cambridge CB3 0DY, England, United Kingdom

This article describes a computational study of viscous effects on lobed mixer flowfields. The computations, which were carried out using a compressible, three-dimensional, unstructured-mesh Navier–Stokes solver, were aimed at assessing the impacts on mixer performance of inlet boundary-layer thickness and boundary-layer separation within the lobe. The geometries analyzed represent a class of lobed mixer configurations used in turbofan engines. Parameters investigated included lobe penetration angles from 22 to 45 deg, stream-to-stream velocity ratios from 0.5 to 1.0, and two inlet boundary-layer displacement thicknesses. The results show quantitatively the increasing influence of viscous effects as lobe penetration angle is increased. It is shown that the simple estimate of shed circulation given by Skebe et al. (Experimental Investigation of Three-Dimensional Forced Mixer Lobe Flow Field, AIAA Paper 88-3785, July, 1988) can be extended even to situations in which the flow is separated, provided an effective mixer exit angle and height are defined. An examination of different loss sources is also carried out to illustrate the relative contributions of mixing loss and of boundary-layer viscous effects in cases of practical interest.

Nomenclature

C_D = dissipation coefficient
C_{Pt} = total pressure loss coefficient
$[C_{Pt}]_{bl}$ = boundary-layer loss coefficient
$[C_{Pt}]_m$ = fully mixed loss coefficient
$[C_{Pt}]_T$ = total loss coefficient (boundary layer + mixing losses)
C_T = thrust coefficient
h = lobe height
h_{eff} = effective lobe height
k = turbulent kinetic energy
M_{sw} = streamwise Mach number
P = static pressure
$\bar{P}^m$ = mass-averaged static pressure
$\bar{P}_T^m$ = mass-averaged total pressure
P_T = total pressure
q = velocity vector, (u, v, w)
r = velocity ratio, U_1/U_2
U_1 = slow-stream velocity at inflow plane
U_2 = fast-stream velocity at inflow plane
u = streamwise velocity
$\bar{u}^m$ = mass-averaged streamwise velocity
v = spanwise velocity
w = transverse velocity
x = streamwise distance
x^* = nondimensional streamwise distance, x/λ
α = lobe penetration angle
α_{eff} = effective lobe penetration angle
Γ_{sw} = streamwise circulation
Γ_{sw}^* = nondimensional streamwise circulation, $\Gamma_{sw}/(\bar{u}^m\lambda)$
δ_d = boundary-layer displacement thickness
ε = turbulent dissipation rate
λ = lobe wavelength
ρ = density

Received Feb. 24, 1994; revision received Oct. 3, 1995; accepted for publication Oct. 15, 1995.

*Graduate Research Assistant, Gas Turbine Laboratory.
†Assistant Professor, Gas Turbine Laboratory. Member AIAA.
‡Professor, Gas Turbine Laboratory. Fellow AIAA.
§Principal Research Engineer, Gas Turbine Laboratory. Member AIAA.
¶Lecturer, Whittle Laboratory. Member AIAA.

I. Introduction

LOBED mixers are fluid mechanic devices used to augment mixing in a variety of applications. Such devices, which have been known since the earliest days of jet engines, received considerable attention during the 1960s when they were used in turbofan engines to reduce jet noise. More recently they have emerged as attractive approaches for mixing core and bypass streams to improve turbofan propulsive efficiency.[2] Lobed mixers are also being studied for use in supersonic mixer ejectors for jet noise reduction at takeoff and landing,[3,4] as well as in combustors for enhancing molecular mixing between fuel and air.

A sketch of a lobed mixer is shown in Fig. 1. There are two different effects associated with the lobed configuration that lead to the increase in mixing rate compared to a flat splitter plate. The first effect is purely geometrical, the increased interfacial length at the trailing edge because of the lobe convolutions. The second is fluid dynamic in nature and is con-

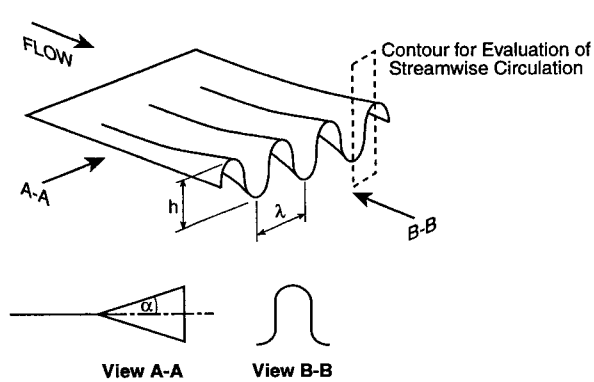

Fig. 1 Lobed mixer.

nected with the existence of the streamwise vorticity shed from the trailing edge of the lobed mixer. Experimental measurements in Paterson[5] and Skebe et al.[1] as well as flow visualization data in Manning[6] indicate that the mixing process is dominated by large-scale (on the order of the lobe height) circulations in the crossflow plane associated with this streamwise vorticity. These large-scale circulations stretch the interface between the streams, increasing both interfacial area and gradients normal to the interface, enhancing the rate of mixing. The experiments reported by Manning,[6] Qiu,[7] and McCormick[8] showed that, for the range of mixer parameters investigated, the increased area between the mixing streams and the crossplane flow associated with the streamwise circulation had roughly equal impact on increasing the rate of mixing.

The experiments referred to were carried out at Mach numbers much less than unity, but the influence of compressibility on lobed mixer performance has also been examined. Compressibility has little impact on the overall flow structure,[9] but does affect the smaller scale mixing that occurs in the shear layers surrounding the interface between the streams. Analogous to the results for planar shear layers,[10] the rate of momentum mixing decreases as the convective Mach number (defined as the relative Mach number of the large-scale structures in the mixing layer with respect to the freestream) increases.

An aspect of lobed mixer flowfields that has received comparatively less attention concerns the influence of viscous effects, although some computations have been carried out using Navier–Stokes solvers.[11,12] The results of the computations and the measurements of Skebe et al.[1] show that under some conditions there can be significant boundary-layer growth in the lobes, filling them with low momentum fluid and decreasing the mixing rate. To date, however, the impact of the inlet boundary layer as well as the boundary layer in the lobe, on overall flow and mixer performance has not been well quantified.

The work described in this article is focused on the influence of viscous effects on lobed mixer performance. In particular, four specific fluid dynamic issues are addressed in this study:

1) As the lobe penetration angle is changed how does the boundary layer in the lobe vary?

2) What is the influence of the boundary layer in the lobe on the magnitude of the streamwise circulation shed from the trailing edge?

3) What is the effect of the inlet boundary layer on the mixing and loss of a lobed mixer?

4) What are the principal lobed mixer loss sources and how do these losses vary with lobe penetration angle and velocity ratio?

II. Research Approach

To answer these questions, a computational investigation was conducted of the flowfield both over the mixer and downstream. The results can be viewed as a numerical experiment in which the aim is to provide generic information about this complex three-dimensional flowfield. While it is clear that present computational procedures cannnot capture all of the aspects of the flow, it is to be stressed that the emphasis here is on global quantities such as circulation and loss. These quantities are predicted sufficiently well to allow useful conclusions to be drawn about these flows.

A. Flow Solver

The computations were carried out using NEWT, a three-dimensional, compressible, unstructured-mesh, Navier–Stokes solver.[13] The code solves the three-dimensional Reynolds-averaged Navier–Stokes equations expressed in strong conservation form, with turbulence being modeled using the k-ε transport equations.[14,15] Low Reynolds number damping terms were used near the walls and the various constants in the k-ε model were given the standard values.[13] The equations of motion in the code are discretized in finite volume form. The primary variables are assumed to have piecewise linear variation over the cell faces between the vertices such that the flux sum for a given cell is evaluated to second-order accuracy in space. Both second- and fourth-difference smoothing are employed, with the level of the former being controlled by the local pressure gradient. The net flux imbalance into each cell is used to update the flow variables by means of a four-step Runge–Kutta time-marching algorithm.

The computational domain is shown in Fig. 2 for a typical mixer configuration. The computations were performed for one-half of a mixer wavelength. The computational grid consisted of unstructured tetrahedral cells and was generated as two separate regions that were matched at their common boundary. The first region was an inviscid grid in which the elements were relatively large and isotropic, and the second consisted of highly stretched boundary-layer elements. The grid was optimized to minimize the dihedral angle of the elements. This procedure was employed to provide the large range in element size and aspect ratio required for modeling viscous lobed mixer flows. A view of the grid at the lobe trailing edge plane is shown in Fig. 3.

The code has been extensively tested for internal flows, particularly those in turbomachinery.[13,16] To assess in more detail the ability to capture mixing processes, the solver was also examined for a constant pressure planar shear layer. This constitutes a severe test of the ability to capture mixing. For this configuration, with a velocity ratio of 0.6, the velocity profiles matched the error-function profile given by Spencer and

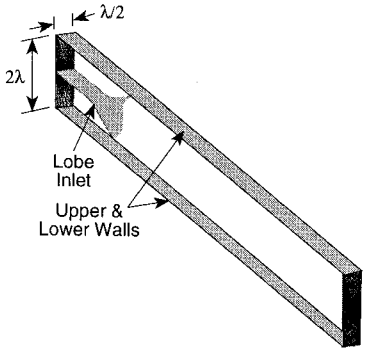

Fig. 2 Computational domain for ADM.

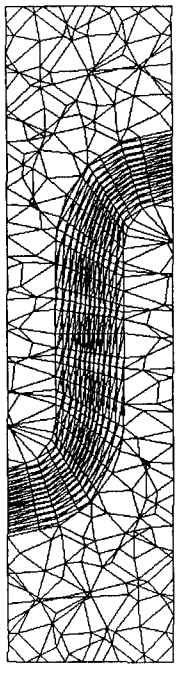

Fig. 3 Computational grid at the mixer trailing edge.

Jones[17] within 6% and the growth rate was within the range of experimental data reported by Spencer and Jones[17] and Dimotakis.[18] Further details of the solver and the grid used can be found in Refs. 16, 19, and 20.

B. Geometries Examined

The investigation focused on a class of lobed mixer geometries, denoted by advanced mixer (ADM), which are typical of advanced mixers considered for use in aircraft propulsion applications. A schematic is shown in Fig. 1. To examine the connection between lobe geometry and streamwise circulation, computations were carried out for mixers with half-angle (or penetration angle) α of 22, 30, 35, and 45 deg. A computation was also carried out on a configuration in which a convoluted plate extension was attached to the trailing edge, as shown in Fig. 4. This configuration, which is denoted as the convoluted plate (CP), has nearly parallel flow at its exit, with essentially no trailing streamwise vorticity. The generation of streamwise circulation can be viewed as a direct consequence of the nonuniform loading in y, and hence, net transverse vorticity on the lobes. The parallel extension, if long enough would have no loading variation along the transverse dimension, no variations in transverse vorticity, and hence, no shed circulation. The convoluted plate represents the limiting case of a mixer in which the lobe angle decreases toward zero at the trailing edge, as do some of those currently in use. It provides insight into the impact of the streamwise circulation and serves as a benchmark for discriminating effects because of the trailing circulation from those due solely to increased trailing-edge length.

The role of velocity ratio was examined by carrying out computations at velocity ratio r, equal to 1.0 and in the range 0.5–0.6. To assess the effect of the inflow boundary layer on the performance of a mixer, two boundary-layer velocity profiles were tested. The majority of the computations were carried out with a uniform total pressure profile at inflow to the computational domain, resulting in a displacement thickness δ^*/λ at the mixer inlet on the order of 0.01 (mixer inlet refers to the beginning of the lobe and not the computational inflow plane). One calculation was carried out with a profile that gave $\delta^*/\lambda \approx 0.25$ at the mixer inlet. Table 1 details the computations that were examined.

Table 1 Parameters examined in mixer computations and nomenclature used

Mixer	α	r	δ^*/λ at inlet
CP (C1)	——	0.4	0.01
ADM (C2)	22	1.0	0.01
ADM (C3)	22	0.5	0.01
ADM (C4)	30	0.5	0.01
ADM (C5)	35	0.5	0.01
ADM (C6)	45	0.63	0.01
ADM (C7)	22	1.0	0.25

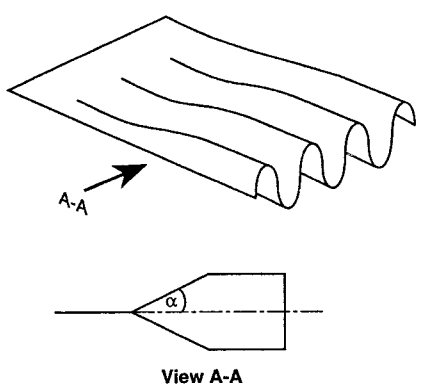

Fig. 4 Convoluted plate.

In all of the computations, the lobe height-to-wavelength ratio h/λ was kept at 1, and so the lobe trailing-edge length was the same for all of the geometries investigated. The stream-to-stream total temperature ratio was 1.0. The geometry and Mach numbers are representative of core and bypass stream mixers in turbofan engines, but the results are also applicable to other flow regimes in which lobed mixers are used, including ejectors and combustors.

III. Features of the Overall Flowfield

A. Generation of Streamwise Circulation and Impact on Mixing

The strength of the streamwise circulation shed from the mixer significantly affects the rate of mixing.[6,7] The nondimensional circulation Γ^*_{sw} is defined as

$$\Gamma^*_{sw} \equiv \frac{1}{\bar{u}^m \lambda} \oint_C \boldsymbol{q} \cdot d\boldsymbol{l} \tag{1}$$

where the integral path is indicated in Fig. 1.

Figure 5 shows the development of Γ^*_{sw}, with axial distance for an ADM and the CP. The penetration angle was 22 deg and the velocity ratios were 0.5 for the ADM and 0.4 for the CP. The generation of streamwise circulation in the lobes differs greatly for the two geometries. For the ADM the circulation begins to rise at the lobe inlet, reaching a value of $\Gamma^*_{sw} \approx 0.7$ at the trailing edge. For the CP, the streamwise circulation at the lobe/extension junction is approximately 40% of that at the trailing edge of the ADM, but between this junction and the trailing edge of the CP, the level of streamwise circulation falls as the flow turns parallel to the freestream. The value of shed circulation is approximately 4% that of the ADM.

The connection between streamwise circulation and downstream flowfield mixing is seen qualitatively in Figs. 6 and 7. These figures show the streamwise Mach number field (denoted M_{sw}) at four downstream axial stations, $x^* = 0$, 1, 3, and 6, where $x^* = x/\lambda$. Figure 6 corresponds to the CP and Fig. 7 to an ADM, both with a penetration angle of 22 deg. For the convoluted plate there is little increase in the length of the interface between the streams and they remain largely unmixed. For the ADM, by $x^* = 1$ the interface has evolved into the characteristic mushroom configuration observed experimentally by Manning[6] and McCormick.[8] Comparing Fig. 7 to Fig. 6 shows the winding-up of the interface that is associated with the streamwise circulation. As stated previously, this winding up increases the interface area and the magnitude of gradients across it, both of which augment mixing rate.

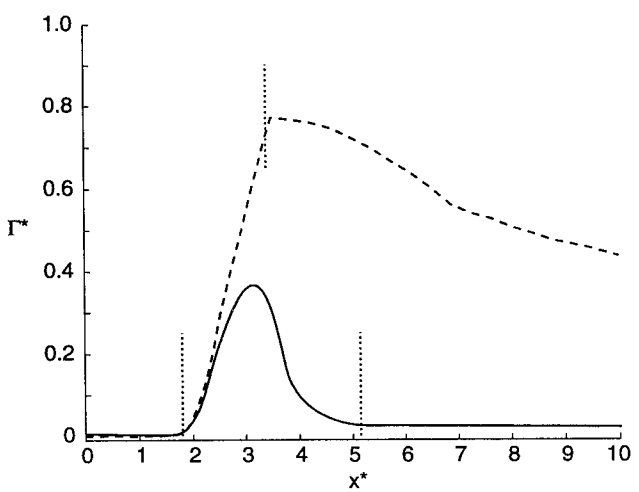

Fig. 5 Γ^*_{sw} vs x^* for ADM (α = 22 deg, r = 0.5) and CP (α = 22 deg, r = 0.4). ——, CP; ---, ADM, and . . . , position of lobe inlet and trailing edges.

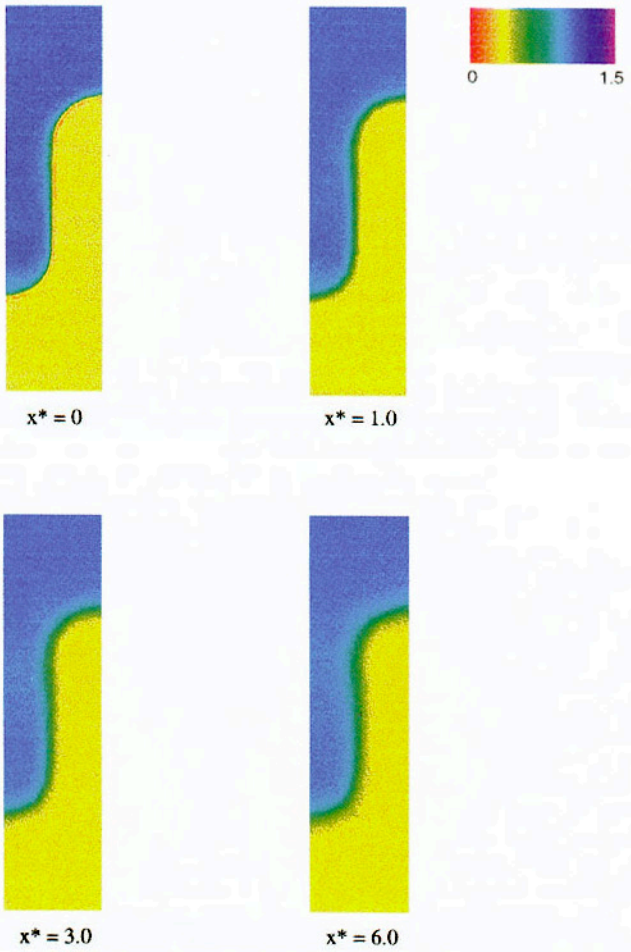

Fig. 6 Mach no. at $x^* = 0$, 1, 3, and 6 for CP ($\alpha = 22$ deg, $r = 0.4$).

B. Effect of Viscosity on Lobed Mixer Flow and Streamwise Circulation

1. *Flowfield Behavior as the Lobe Penetration Angle is Varied*

As the lobe penetration angle is increased the behavior of the flow in the lobe is altered because boundary-layer blockage, and then separation, become progressively more important. For a penetration angle of 22 deg, the computations showed no flow separation. For a 35-deg lobe angle, separation was observed close to the trailing edge and along the vertical wall of the lobe in the low-velocity stream. For a 45-deg lobe, extensive separation was seen from halfway through the lobe to the trailing edge.

2. *Streamwise Circulation Magnitude*

For lobed mixers with no separation and little boundary-layer blockage, Skebe et al.[1] have shown that a good estimate of the trailing streamwise circulation is obtained if one assumes that the fluid leaves the mixer at α. If so, Γ_{sw} is given by

$$\Gamma_{sw} \approx 2\bar{u}^m h \tan \alpha \tag{2}$$

or nondimensionally as

$$\Gamma^*_{sw} \approx 2(h/\lambda)\tan \alpha \tag{3}$$

As the lobe penetration angle is increased, or if the inflow boundary layer is appreciable compared to the lobe height, the assumptions that underlie Eqs. (2) and (3) are less valid. The computations provide a way to assess the utility of these expressions in situations without the restrictions that these assumptions imply.

In Fig. 8 a comparison of the estimated circulation from Eq. (3) and that derived from the computational results is shown. For lobe penetration angles of 30 deg or more, Eq. (3) overpredicts the circulation by progressively larger amounts, and for the largest angle, 45 deg (denoted as C6 in Fig. 8), there is a factor of 2 difference between the computations and the simple estimate. The difference arises from the increased thickness of low-velocity fluid because of the boundary layer and separated flow in the lobe, which reduces the effective lobe angle and height.

To assess this effect, it is useful to examine δ^*, defined as

$$\delta^* = \int_0^\delta \left[1 - \frac{\rho u}{(\rho u)_{max}}\right] dz \tag{4}$$

The computed displacement thickness at the lobe trough and peak, for lobe inlet and trailing-edge stations (Fig. 9a), can be used to estimate α_{eff} and h_{eff} for each side of the lobed mixer, as illustrated schematically in Fig. 9b. These values can then be employed to give a modified version of Eq. (3), which links the trailing streamwise circulation to the actual (fluid) angles at the lobe exit, rather than the geometry alone. This is

$$\Gamma^*_{sw} \approx (h_{eff,1}/\lambda)\tan(\alpha_{eff,1}) + (h_{eff,2}/\lambda)\tan(\alpha_{eff,2}) \tag{5}$$

Figure 10 shows comparisons of computed circulations and those given by Eq. (5). The agreement is within 5%, even for the 45-deg lobe case in which there was substantial flow separation (C6 in Fig. 10).

It should also be noted from Figs. 8 and 10 that, for the class of lobe geometries tested, there is no benefit in increasing the lobe penetration angle above 30 deg. For penetration an-

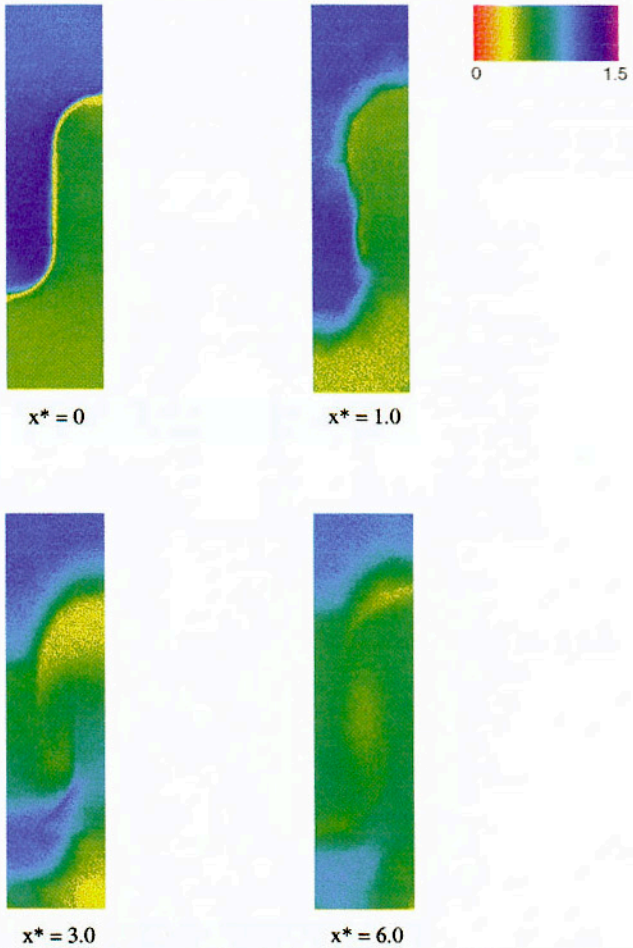

Fig. 7 Mach no. at $x^* = 0$, 1, 3, and 6 for ADM ($\alpha = 22$ deg, $r = 0.5$).

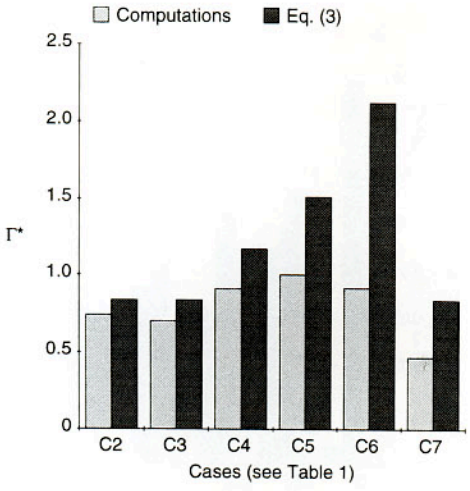

Fig. 8 Streamwise circulation based on penetration angle.

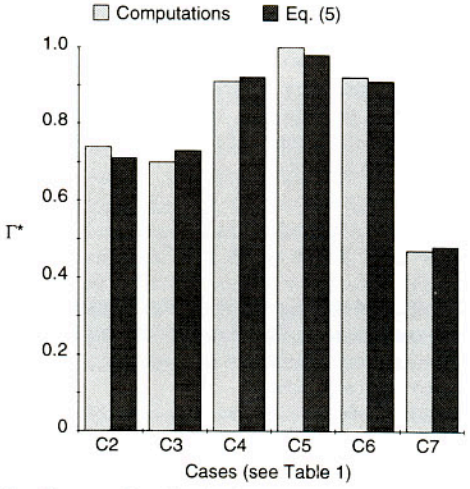

Fig. 10 Streamwise circulation based on effective angle.

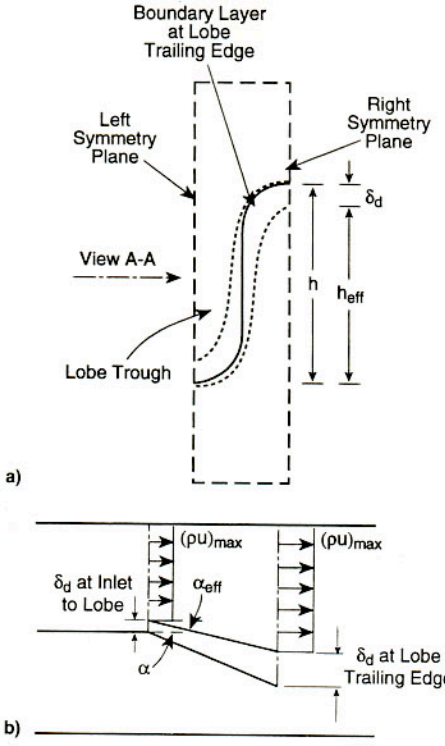

Fig. 9 Boundary-layer blockage and definition of α_{eff}: a) schematic of boundary-layer profile at the lobe trailing edge and b) view A-A.

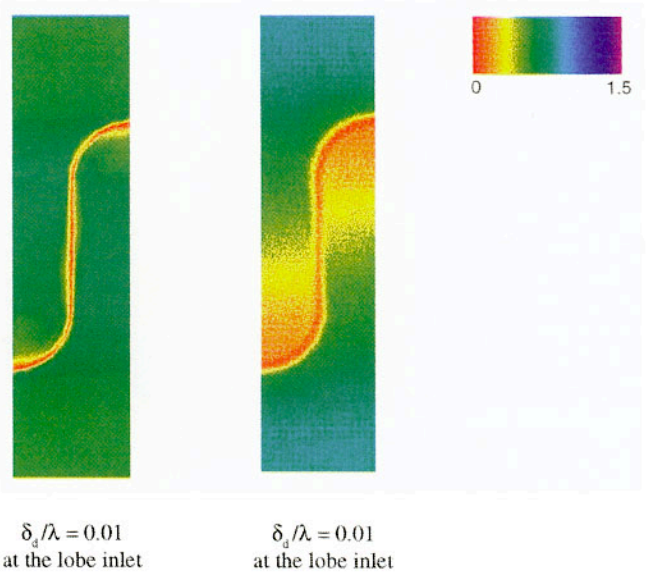

Fig. 11 Mach no. at the lobe trailing edge for $\delta_d/\lambda = 0.1$ and 0.25 at the lobe inlet ($r = 1.0$).

gles larger than 30 deg, the level of shed streamwise circulation becomes limited by viscous effects and eventually is reduced when large-scale separation occurs in the lobe troughs.

3. *Effect of Inlet Boundary Layer*

The computations described in the previous section were carried out with a thin displacement thickness of $\delta^*/\lambda \approx 0.01$ at the lobe inlet. To consider the impact of displacement thickness a case was computed with a value of $\delta^*/\lambda \approx 0.25$ at the lobe inlet.

Figure 11 shows the Mach number field at the lobe trailing edge for the two different inlet displacement thicknesses. The velocity ratio is equal to 1.0. With $\delta^*/\lambda \approx 0.25$, a considerable portion of the lobe was filled with low-momentum fluid, and the trailing circulation was reduced by approximately 35% compared to the case with $\delta^*/\lambda \approx 0.01$ (comparing cases C2 and C7 in Fig. 10). The simple estimate for circulation based on Eq. (5), using the effective penetration angles and heights, is in good agreement with the computed circulation, differing by less than 2%.

IV. Losses in Lobed Mixers

An important question connected with mixing enhancement from the streamwise vorticity is the penalty associated with the increased mixing rate. Because the trailing circulation is closely related to the mixing augmentation,[6-9] it is of interest to characterize the loss incurred because of the trailing circulation compared to other loss in the overall process.

The total losses that occur in lobed mixer configurations can be divided into two categories:

1) *Boundary-layer losses*, i.e., losses having to do with wetted surfaces. This includes losses on the lobe surface, as well as on the shrouds that correspond to the lower and upper walls of the computational domain (e.g., see Fig. 2).

2) *Mixing losses*, containing contributions from the mixing out of nonuniformities associated with the velocity field exiting the lobes. While this includes the wake flow caused by the lobe boundary layer and the trailing edge, the most important contribution is generally the mixing of the freestream nonuniformity of flow outside these thin layers.

Assessments of losses were made as a function of velocity ratio, keeping the trailing circulation constant (fixed penetration angle and lobe trailing-edge geometry), and as a function

of lobe penetration angle, keeping the velocity ratio fixed. An examination of the relation between total pressure loss and thrust decrease was also carried out. In the discussion that follows the total pressure losses are expressed in the form of a loss coefficient, denoted C_{Pt}, in which the loss is nondimensionalized by the difference between the mass-averaged inflow total and static pressures, i.e.,

$$C_{Pt} \equiv \frac{\Delta P_T}{(\bar{P}_T^m - \bar{P}^m)_{\text{inflow}}} \tag{6}$$

A constant area mixing process was employed to calculate the fully mixed out loss. The flowfield at the lobe trailing edge was used as inflow conditions to a control volume and then mixed out to uniform flow.

The boundary-layer losses were estimated using an empirical relationship described by Cumpsty,[21] which relates entropy production in the boundary layer to the integral of the cube of the local freestream velocity, i.e.,

$$\text{mass flow-weighted total pressure loss} = C_D \int U^3 \, dA \tag{7}$$

For turbulent boundary layers the C_D is not a strong function of Reynolds number and a value of 0.002 was taken as representative.[21] For the constant total temperature mixing process simulated in this study, this entropy-based parameter can be directly related to the change in total pressure.

The shroud boundary-layer loss was taken as the loss because of the boundary layers on the upper and lower walls of the computational domain; in practice, the value of this loss will depend on the particular shroud geometry used. The flowfield near the shroud is dependent on the distance between the shroud and mixer. For this study, the upper and lower walls were one-half lobe wavelength from the peak of the mixer.

A. Effect of Velocity Ratio on Loss

To assess the effect of velocity ratio, the loss for the ADM with a penetration angle of 22 deg was computed for velocity ratios of 1.0 and 0.5 (cases C2 and C3). The (nondimensional) trailing circulations were within 1% of one another for these configurations. The boundary-layer loss coefficient and the mixing loss coefficient results are given in Figs. 12 and 13, respectively. Relative contributions to the overall loss coefficient are shown in Fig. 14. The lobe and shroud boundary-layer losses for the two cases were different by only 10%, but there was approximately three times more mixing loss for the case with velocity ratio of 0.5.

With a velocity ratio of 1.0, the contribution of the boundary layer and mixing losses to the total loss were approximately equal (within 20%). The main loss was the loss associated with the shroud boundary layers, which was roughly four times the lobe boundary-layer loss, reflecting primarily the difference in surface area between the lobe and shroud.

For a velocity ratio of 0.5, mixing losses accounted for more than 80% of the total loss. For typical velocity ratios encountered in practice, therefore (which tend to be 0.5 or less), mixing losses downstream of the lobe trailing edge will typically be the largest contribution to the total loss incurred.

In Fig. 12 the losses in the boundary layers on the high-velocity shroud for the CP were approximately 20 times the low-velocity shroud values (case C1). For the CP there was limited mixing and the low- and high-velocity streams remained close to the shroud along the complete axial extent of the computational domain (see Fig. 6). In contrast, for the ADM (see Fig. 7), there was rapid mixing downstream of the trailing edge, resulting in the velocities near the shrouds being more closely matched. Because of this, the low- and high-velocity shroud boundary-layer losses were of similar magnitude.

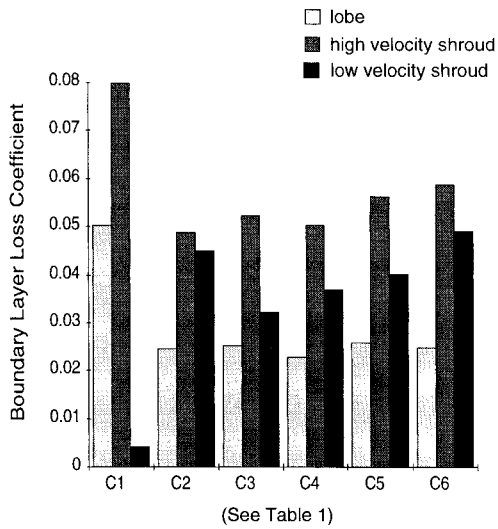

Fig. 12 Boundary-layer loss coefficient.

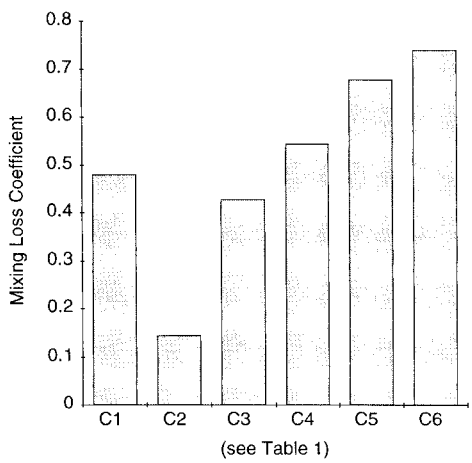

Fig. 13 Mixing loss coefficient.

B. Effect of Penetration Angle on Losses

Figure 12 shows loss results for lobe penetration angles of 22, 30, 35, and 45 deg (cases C2, C3, C4, C5, respectively). Increasing the lobe penetration angle caused an increase in the boundary-layer losses because of the higher local velocities due to increased streamline curvature; as Eq. (7) shows, the boundary-layer losses scale with the cube of the freestream velocity. Figure 13 shows the mixing losses, based on the control volume analysis. Mixing loss increased with penetration angle at over twice the rate of the boundary layer loss. For $\alpha = 22$ deg (C3) the mixing loss coefficient was approximately 0.43, increasing to 0.74 for $\alpha = 45$ deg (C6).

Several different mechanisms contribute to mixing loss. One of these is the kinetic energy that is associated with velocity components normal to the mean flow direction (axial). The normal components of velocity are introduced by the lobed mixer. If one regards the kinetic energy of the normal velocities as totally lost, this portion of the loss would scale with $\sin^2\alpha_{\text{eff}}$. Following these assumptions, the loss because of kinetic energy of normal velocities accounts for 80% of the mixing loss for the ADM with $r = 1.0$ and thin boundary layers ($\alpha_{\text{eff}} \approx \alpha = 22$ deg). For the cases with a velocity ratio of 0.5, however, there is a larger contribution to the mixing loss from the mixing out of the nonuniform streamwise velocities. Based on the scaling suggested earlier, for a velocity ratio of 0.5 the mixing of the normal velocities accounted for less than 30% of the mixing loss.

For flow regimes in which the displacement thickness is small and the geometric lobe angle and the effective angle are

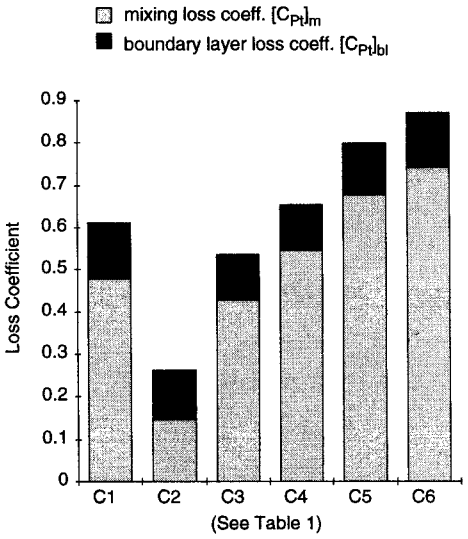

Fig. 14 Contributions to the overall loss coefficient.

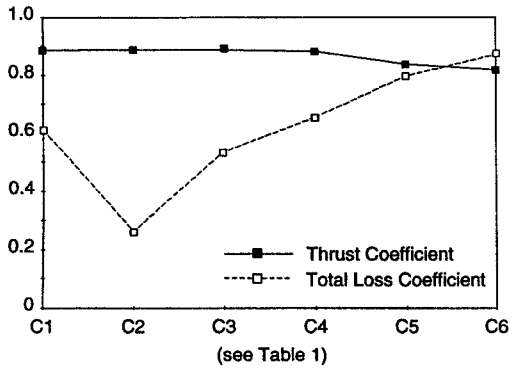

Fig. 15 Total loss coefficient and thrust coefficient.

close to one another, the losses associated with the normal velocity components introduced by the lobe can be regarded to good approximation as scaling with $\sin^2\alpha$. However, the computations show that as the penetration angle is increased past 22 deg, it is boundary-layer blockage and separation that are associated with the increase in mixing loss, rather than swirl. In fact, for the three largest lobe angles the effective penetration angles were virtually the same at 26, 26.5, and 25 deg, while the mixing loss continued to increase with increasing metal angle.

C. Overall Total Pressure Loss and Thrust Loss

The thrust coefficient C_T is defined as the ratio of the momentum flux of the coflowing streams if mixed out to a static pressure equal to the inflow static pressure (denoted F_{mix}), to the momentum flux of the unmixed streams at the inflow (denoted F_{inflow}), i.e.,

$$C_T = F_{mix}/F_{inflow} \tag{8}$$

where F_{inflow} and F_{mix} are defined as follows:

$$F_{inflow} = \int_{flow\ area} (\rho u^2)_{inflow}\, dA \tag{9}$$

$$F_{mix} = \int_{flow\ area} [(P + \rho u^2)_{te} - P_{inflow}]\, dA \tag{10}$$

The subscript te, in Eqs. (8–10), denotes the lobe trailing-edge plane.

Figure 15 shows C_T and $[C_{Pt}]_T$ (boundary layer plus mixing losses), for the different mixer configurations. The range of thrust coefficient is approximately 8%, from 0.888 to 0.818.

For the ADM configurations, a trend of reduced thrust coefficient with increasing lobe penetration angle is evident. For smaller penetration angles this occurs because of the larger normal components of velocity (and, hence, large kinetic energy) at the trailing edge, but, for the configurations examined, above α = 22 deg, the effect is because of boundary-layer blockage and separation. The thrust coefficients were the highest for the CP and ADM with α = 22 deg. Despite having parallel flow at its trailing edge, the CP had the same thrust coefficient as the ADM because of the additional drag over its extension, which quadrupled the mixer's wetted area.

V. Summary and Conclusions

1) A compressible, three-dimensional Navier–Stokes solver was used to study the flowfield generated by a lobed mixer nozzle. The code, which captured the experimentally observed features of the flow, was applied to provide insight and quantitatively assess the impact of viscous effects on mixer performance.

2) Lobe geometries were examined with different penetration angles ranging from 22 to 45 deg. Flow separation first occurred at a penetration angle of 35 deg. For the range of mixer parameters examined, there was no benefit, in terms of the creation of trailing streamwise circulation, of increasing the penetration angle above 30 deg because of increased boundary-layer blockage and flow separation.

3) As the lobe penetration angle was increased the trailing circulation deviated from a simple one-dimensional estimate[1] because of increased boundary-layer blockage and eventually flow separation. The one-dimensional approach, however, was shown to provide an accurate estimate of the trailing streamwise circulation, even for separated flow, if one formulates it in terms of an effective penetration angle and effective lobe height.

4) The performance of the lobed mixer was dependent on the characteristics of the inlet boundary layer. A thick inlet boundary layer led to filling of the lobe trough with low-momentum fluid, resulting in a reduced lobe effective angle, and hence, reduced streamwise circulation, compared to a configuration with a thin inlet boundary layer. This behavior could also be quantified using the effective lobe angle and height described previously.

5) For a velocity ratio of unity, boundary layer and mixing losses were comparable, but for realistic velocity ratios (0.5 or less) mixing losses were dominant, accounting for approximately 80% of the total loss.

6) For fixed velocity ratio, as lobe penetration angle was increased, total pressure loss increased and the thrust decreased. For lobe penetration angles less than 30 deg, the variation in loss with penetration angle was mainly because of loss of kinetic energy associated with the swirl imparted to the streams. For larger penetration angles, additional swirl was not introduced; however, losses continued to increase because of retardation and eventually separation of flow in the lobe troughs.

Acknowledgments

Support for this work was provided by NASA Contract NAG3-1364, with supervision by James R. De Bonis and Colin Drummond; and Naval Air Systems Command Contract N0001988-C0029 with supervision by George Derderian and Lewis Sloter II. Both of these sources of support are gratefully acknowledged. The authors would also like to acknowledge the many stimulating discussions with N. A. Cumpsty of Cambridge and F. E. Marble of the California Institute of Technology, and the generous and effective assistance with grid generation from Jaime Peraire of the Massachusetts Inst. of

Technology. In addition, the authors would like to thank T. J. Barber and D. C. McCormick of the United Technologies Research Center for help on a number of topics.

References

[1]Skebe, S. A., Paterson, R. W., and Barber, T. J., "Experimental Investigation of Three-Dimensional Forced Mixer Lobe Flow Fields," AIAA Paper 88-3785, July 1988.

[2]Little, D. R., "Fuel-Efficient-5C Long Duct Mixed Flow Nacelle," *The Leading Edge*, GE Aircraft Engines, Cincinnati OH, 1993.

[3]Lord, W. K., Jones, C. W., Stern, A. M., Head, V. L., and Krejsa, E. A., "Mixer Ejector Nozzle for Jet Noise Suppression," AIAA Paper 90-1909, July 1990.

[4]Tillman, T. G., Paterson, R. W., and Presz, W. M., "Supersonic Nozzle Mixer Ejector," *Journal of Propulsion and Power*, Vol. 8, No. 2, 1992, pp. 512–519.

[5]Paterson, R. W., "Turbofan Forced Mixer-Nozzle Internal Flowfield: Volume 1—A Benchmark Experimental Study," *Journal of Engineering for Gas Turbines and Power*, Vol. 106, July 1984, pp. 692–698.

[6]Manning, T. A., "Experimental Study of Mixing Flows with Streamwise Vorticity," M.S. Thesis, Massachusetts Inst. of Technology, Cambridge, MA, 1991.

[7]Qiu, Y. J., "A Study of Streamwise Vortex Enhanced Mixing in Lobed Mixer Devices," Ph.D. Dissertation, Massachusetts Inst. of Technology, Cambridge, MA, 1992.

[8]McCormick, D. C., "Vortical and Turbulent Structure of Planar and Lobed Mixer Free Shear Layers," Ph.D. Dissertation, Univ. of Connecticut, Storrs, CT, 1992.

[9]Elliot, J. K., "A Computational Investigation of the Fluid Dynamics of a Three-Dimensional, Compressible, Mixing Layer with Strong Streamwise Vorticity," M.S. Thesis, Massachusetts Inst. of Technology, Cambridge, MA, 1990.

[10]Papamoschou, D., and Roshko, A., "The Compressible Turbulent Shear Layer: An Experimental Study," *Journal of Fluid Mechanics*, Vol. 197, Feb. 1988, pp. 452–477.

[11]Koutmos, P., McGuirk, J. J., Priddin, C. H., and Sodha, M. N., "Numerical Investigation of the Flow Within a Turbofan Lobed Mixer," *Journal of Propulsion and Power*, Vol. 7, No. 3, 1981, pp. 389–394.

[12]Koutmos, P., and McGuirk, J. J., "Turbofan Forced Mixer/Nozzle Temperature and Flow Field Modeling," *International Journal of Heat and Mass Transfer*, Vol. 32, No. 6, 1989, pp. 1141–1159.

[13]Dawes, W. N., "The Practical Application of Solution-Adaptation to the Numerical Simulation of Complex Turbomachinery Problems," *Progress in Aerospace Sciences*, Vol. 29, No. 3, 1992, pp. 221–269.

[14]Lam, C. K. G., and Bremhorst, K. A., "Modified Form of the k-ε Model for Predicting Wall Turbulence," *Journal of Fluids Engineering*, Vol. 103, 1981.

[15]Patel, V. C., Rodi, W., and Scheuerer, G., "Turbulence Models for Near-Wall Flows and Low Reynolds Numbers: A Review," *AIAA Journal*, Vol. 23, No. 9, 1984.

[16]Dawes, W. N., "The Simulation of Three-Dimensional Viscous Flow in Turbomachinery Geometries Using a Solution-Adaptive Unstructured Mesh Methodology," *Journal of Turbomachinery*, Vol. 114, No. 3, 1992, pp. 528–537.

[17]Spencer, B. W., and Jones, B. G., "Statistical Investigation of Pressure and Velocity Fields in the Turbulent Two-Stream Mixing Layer," AIAA Paper 71-613, June 1971.

[18]Dimotakis, P., "Turbulent Free-Shear Layer Mixing," AIAA Paper 89-0262, Jan. 1989.

[19]Krasnodebski, J. K., "Numerical Investigations of Lobed Mixer Flow Fields," M.S. Thesis, Massachusetts Inst. of Technology, Cambridge, MA, 1995.

[20]O'Sullivan, M. N., "A Computational Study of the Effects of Viscosity on Lobed Mixer Flowfields," M.S. Thesis, Massachusetts Inst. of Technology, Cambridge, MA, 1993.

[21]Cumpsty, N. A., *Compressor Aerodynamics*, Longman Group, Essex, England, UK, 1989, pp. 21–34, Chap. 1.